Precision RNAi using synthetic shRNAmir target sites

Thomas Hoffmann[1,2,5,#], Alexandra Hörmann[3,#], Maja Corcokovic[3,#], Jakub Zmajkovic[1], Matthias Hinterndorfer[1], Jasko Salkanovic[3], Fiona Spreitzer[3], Anna Köferle[3], Katrin Gitschtaler[3], Alexandra Popa[3], Sarah Oberndorfer[3], Florian Andersch[1], Markus Schäfer[1], Michaela Fellner[1], Nicole Budano[3], Jan G. Ruppert[3], Paolo Chetta[3], Melanie Wurm[3], Johannes Zuber[1,4*] & Ralph A. Neumüller[3*]

[1] Institute of Molecular Pathology (IMP), Campus-Vienna-Biocenter 1, 1030 Vienna, Austria

[2] Vienna BioCenter PhD Program, Doctoral School of the University at Vienna and Medical University of Vienna, Vienna BioCenter (VBC), 1030 Vienna, Austria

[3] Boehringer Ingelheim RCV GmbH & Co KG, Doktor-Boehringer-Gasse 5-11, 1120 Vienna, Austria

[4] Medical University of Vienna, Vienna BioCenter, 1030 Vienna, Austria

[5] Present address: Advantage Therapeutics GmbH, Karl-Farkas-Gasse 22, 1030 Vienna, Austria

[#] These authors contributed equally to this work

[*] Corresponding authors: J.Z.: johannes.zuber@imp.ac.at; R.A.N.: ralph.neumueller@boehringer-ingelheim.com

Abstract

Loss-of-function genetic tools are widely applied for validating therapeutic targets, but their utility remains limited by incomplete on- and uncontrolled off-target effects. We describe artificial RNA interference (ARTi) based on synthetic, ultra-potent, off-target-free shRNAs that enable efficient, inducible, and reversible suppression of any gene upon introduction of a synthetic target sequence into non-coding transcript regions. ARTi establishes a scalable loss-of-function tool with full control over on- and off-target effects.

Results and Discussion

Drug development is guided by genetic loss-of-function (LOF) experiments that validate a therapeutic target, study its general and disease-specific functions, and thereby model and benchmark expected activities of inhibitory molecules. Applied genetic tools include RNAi, CRISPR/Cas9, and site-specific recombination technologies such as the Cre-Lox or Flp-FRT systems[1,2]. While these technologies have undoubtedly revolutionized genetic screening, target identification and validation, each method is associated with drawbacks that limit the usability for certain aspects of target validation. Specifically, RNAi is prone to off-target effects[3–5] and insufficient knock-down levels, while CRISPR/Cas9-based methods are associated with off-target effects and incomplete LOF across cell populations. These limitations are particularly problematic for candidate targets in oncology, which should ideally be validated genetically

in cancer cell lines and tumor models *in vivo*. In both cases, insufficient LOF or off-target effects can lead to far-reaching misconceptions about target suppression effects. Outgrowth of wild-type clones that retain gene function upon CRISPR- and recombination-based gene editing can result in transient phenotypes that complicate data interpretation. Similarly, insufficient knock-down or uncontrolled off-target effects induced by RNAi can lead to an unjustified de-prioritization or pursuit of candidate targets, respectively. Prior to initiating the time- and resource-intense process of drug development, more informative target validation assays would be highly desirable.

To develop such an assay system, we reasoned that instead of using gene-specific loss-of-function triggers for every new candidate gene, the expression of any gene could be efficiently suppressed by engineering the target site of a pre-validated, highly potent, synthetic short-hairpin RNA (shRNA) into its exonic sequence (Fig. 1a). Besides ensuring efficient target knockdown in a highly standardized manner, such an approach would also provide full control over off-target activities through expressing the shRNA side-by-side in target-site engineered and wildtype cells. As suitable RNAi system, we chose optimized micro-RNA embedded shRNAs (shRNAmirs) in the miR-E backbone[6], which do not interfere with endogenous miRNA processing[7] and can be expressed from tet-responsive elements and other Pol-II promoters in the 3'-UTR of fluorescent reporter genes, thus providing a versatile system for inducible RNAi[8]. To identify potent artificial RNAi (ARTi) triggers with minimal off-target activity, we analyzed the nucleotide composition of shRNAs that reach exceptionally high performance scores in common shRNA design algorithms[9] and of miRNA seed sequences with exceptionally low off-target scores according to siSPOTR[10]. By merging nucleotide biases identified in both analyses, we derived a 22-nt base composition matrix for the design of ARTi shRNAmirs (TTCGWWWNNAHHWWCATCCGGN; W = A/T, H = A/T/C; N = A/T/G/C) (Fig. 1b; Extended Data Fig. 1a,b). To further reduce possible off-target effects, we eliminated all shRNAs whose extended seed sequence (guide positions 2-14) had a perfect match in the human or mouse transcriptome and, finally, selected six top-scoring ARTi predictions for experimental validation.

We tested these ARTi-shRNAmirs using an established knockdown reporter assay[6] for their ability to suppress expression of a GFP transgene that harbors the respective target sites in its 3'-UTR. In all six cases, ARTi-shRNAmir matched or outperformed previously validated highly potent shRNAmirs targeting Renilla luciferase or PTEN[6] (Extended Data Fig. 1c). We compared these results to a panel of 592 gene-specific shRNAs that were tested using the same assay and found that ARTi-shRNAmirs ranked among top-performing shRNAmirs overall (Fig. 1c). Next, we selected the three top-performing ARTi-shRNAmirs and evaluated possible off-target activities using competitive proliferation assays and transcriptome profiling. ARTi-shRNAmir expression had no effects on proliferation or survival in four human and three mouse cell lines (Fig. 1d, Extended Data Fig. 1d), with the exception ARTi.6634 which induced a mild fitness defect in the murine leukemia cell line RN2. In contrast to effects of a MEK inhibitor trametinib, which we included as a positive control, stable expression of ARTi-shRNAmirs had only marginal effects in RNA-sequencing in two commonly used human cell lines (Fig. 1e, f, Extended Data Fig. 1e,f) and no effect in proliferation assays (Extended Data Fig. 1g), indicating that they do not trigger major off-target effects, even in the absence of their respective target site. Together, these studies established a set of highly potent, off-target-free ARTi-shRNAmirs, among which we selected ARTi.6570 (ARTi-shRNAmir) for further investigations.

To establish ARTi as a method for target validation, we performed ARTi-based LOF experiments in cancer cell lines and xenograft models for three prominent oncology targets: EGFR and KRAS, which act as driving oncogenes in various cancer types[11,12], and STAG1, which has been identified as a synthetic lethal

interaction with recurrent loss-of-function mutations of STAG2[13–16]. To establish an ARTi-repressible version of oncogenic EGFR^{del19}, we cloned ARTi-shRNAmir target sequences into an expression construct encoding EGFR^{del19} fused to dsRed (Fig. 2a), which rendered Ba/F3 cells cytokine-independent and sensitive to EGFR inhibition (Extended Data Fig. 2a). We introduced this construct into human EGFR^{del19}-dependent PC-9 lung adenocarcinoma cells and subsequently knocked out the endogenous *EGFR* gene. The EGFR^{del19}::dsRed::ARTi transgene fully rescued the loss of endogenous EGFR^{del19}, while doxycycline (Dox)-induced expression of the ARTi-shRNAmir (ARTi.6570) strongly inhibited proliferation of PC-9 cells and triggered a near-complete suppression of the EGFR^{del19}::dsRed protein (Fig. 2b,c ; Extended Data Fig. 2b). Consistently, in RNA-sequencing we observed an almost complete drop of reads mapping to the codon-optimized *EGFR^{del19}::dsRed::ARTi* transgene upon dox-inducible expression of the ARTi-shRNAmir, as well as a downregulation of *DUSP6* and other canonical targets of RAF-MEK-ERK signaling, which acts as key effector pathway of EGFR^{del19} (Extended Data Fig. 2c-e).

To evaluate whether ARTi can recapitulate drug activities *in vivo*, we xenotransplanted *EGFR^{del19}::dsRed::ARTi* engineered PC-9 cells harboring the Dox-inducible ARTi-shRNAmir and treated recipient mice upon tumor formation with either Dox or the clinically approved EGFR inhibitor Osimertinib. Dox-induced expression of the ARTi-shRNAmir led to rapid and durable tumor regression that was indistinguishable from the effects of Osimertibib (Fig. 2d) and not observed in parental PC-9 cells that lack the ARTi target site (Extended Data Fig. 2f). Thus, ARTi-induced phenotypes can be unambiguously attributed to on-target effects that predict the activity of advanced small-molecule inhibitors *in vivo*.

In a second study, we used ARTi to investigate KRAS^{G12R}, an oncogenic variant of KRAS for which *in-vivo* compatible inhibitors do not yet exist. To establish a suitable KRAS^{G12R}-driven model, we engineered a *dsRed::KRAS^{G12R}::ARTi* transgene and the dox-inducible ARTi-shRNAmir into KRAS^{G12C}-dependent MIA PaCa-2 pancreatic adenocarcinoma cells and subsequently knocked out endogenous KRAS alleles (Fig. 2e, Extended Data Fig. 3a). As expected, switching the driving oncogene from KRAS^{G12C} to KRAS^{G12R} rendered MIA PaCa-2 cells resistant to the KRAS^{G12C} inhibitor AMG-510[17–19] (Extended Data Fig. 3b). ARTi-shRNAmir induction led to strong suppression of dsRed::KRAS^{G12R} expression at the mRNA and protein level (Fig. 2f, Extended Data Fig. 3c,d) and marked anti-proliferative effects (Fig. 2g). In xenograft experiments, ARTi-mediated suppression of KRAS^{G12R} led to full tumor regression in the absence of KRAS^{G12C} (Fig. 2h), while tumors harboring both oncogenic KRAS alleles only displayed a delay in tumor progression, suggesting that both oncogenes contribute to tumorigenesis *in vivo*.

To evaluate STAG1 as synthetic-lethal dependency that is relevant in wide range of STAG2-deficient cancers (Extended Data Fig. 4a)[13–16], we engineered an isogeneic pair of STAG2-wildtype and -deficient HCT-116 colon carcinoma cells and homozygously inserted ARTi target sites into the 3'-UTR of endogenous *STAG1* (Fig. 2i). Western blotting confirmed the knockout of *STAG2*, the homozygous insertion of the targeting cassette into the *STAG1* locus, and potent suppression of STAG1 following Dox-induced ARTi-shRNAmir expression (Fig. 2j,k; Extended Data Fig. 4b). Suppression of STAG1 in STAG2-deficient HCT-116 cells impaired their proliferation *in vitro* (Extended Data Fig. 4c) and the progression of xenografted tumors *in vivo* (Fig. 2l), while Dox-induced expression of the ARTi-shRNAmir had no anti-proliferative effects in the presence of STAG2.

Together, these studies establish ARTi as a versatile and precise LOF method for target validation in oncology and beyond. Instead of designing gene-specific LOF reagents that remain prone to off-target effects, ARTi involves a simple, highly standardized experimental procedure that provides full control over

121 on- and off-target effects and can be applied to any coding and non-coding gene. In cells that are pre-
122 engineered to express the Dox-inducible ARTi-shRNAmir, candidate genes can be converted into ARTi
123 target genes and subsequently evaluated head-to-head in a highly standardized manner, either through
124 knocking in ARTi target sites into endogenous loci or through knock-out rescue approaches. Placement of
125 ARTi target sites in non-coding transcript regions leaves the endogenous target protein unaltered, which
126 is a key advantage over chemical-genetic LOF methods relying on the introduction of degron tags[20,21].
127 Through engineering multiple target sites in the same cell, in principle ARTi enables combinatorial LOF
128 perturbations, e.g. for modeling synergistic target interactions, without multiplying the risk for off-target
129 effects. Beyond providing a scalable method for early target validation, we foresee that ARTi can be used
130 to establish on-target benchmark phenotypes for guiding the development and optimization of inhibitory
131 molecules.

132

133 **Figure Legends**

134

135 **Figure 1 | Design and selection ARTi-shRNAmirs. A,** Schematic outline of the ARTi approach. **B,** Sequence
136 logo (https://weblogo.berkeley.edu) displaying nucleotide position biases of 2161 shRNAs with
137 exceptionally high DSIR scores (>105). Inlay depicts miRNA seed sequence biases. **C,** Reporter assay
138 comparing gene-specific shRNAs to ARTi-shRNAmirs. **D,** Competitive proliferation assays in human cell
139 lines after transduction with ARTi-shRNAmirs, neutral (shRen.713) and essential control shRNAs
140 (shRPL9.324 or shPSMA3.164). **E,** Principal component (PC) analysis of gene expression profiling upon
141 stable expression of indicated shRNAs or treatment with MEK inhibitor (trametinib) in RKO cells. **F,**
142 Volcano plots visualizing de-regulated genes upon expression of indicated shRNAs and trametinib
143 treatment in RKO cells, compared to empty vector control.

144

145 **Figure 2 | Experimental validation of the ARTi approach. A,** Schematic of EGFR^{del19}-ARTi engineering in
146 PC-9 cells. Blue color denotes overexpressed ARTi variant. Green denotes endogenous gene. **B,** Western
147 Blot demonstrating knock-down of EGFR^{del19}-ARTi. Western Blot is a representative example of three
148 independent biological repeat experiments. **C,** Proliferation assay and crystal violet staining of parental
149 and engineered PC-9 cells in absence or presence of Dox. Crystal violet staining is a representative
150 example of two independent biological repeat experiments. **D,** *In vivo* experiment comparing Dox-induced
151 EGFR^{del19}-ARTi knockdown to pharmacological EGFR^{del19} inhibition. Mean tumor volume and +/- s.e.m. is
152 plotted for all *in vivo* experiments. **E,** Schematic of MIA PaCa-2 engineering. Blue color denotes
153 overexpressed ARTi variant. Green denotes endogenous gene. **F,** Western blot for KRAS and Actin in
154 indicated engineered MIA-PaCa-2 cells in the presence and absence of Dox. Western Blot is a
155 representative example of two independent biological repeat experiments. **G,** Proliferation assay and
156 crystal violet staining of parental and engineered MIA PaCa-2 cells in absence or presence of Dox. Crystal
157 violet staining is a representative example of two independent biological repeat experiments. **H,** Growth
158 curves of tumors implanted with engineered MIA PaCa-2 cells in absence and presence of Dox. In vivo **I,**
159 Schematic of C-terminal endogenous tagging of STAG1. Green color denotes endogenous genes. **J,**
160 Western Blot demonstrating knock-down of STAG1-ARTi. Western Blot is a representative example of
161 three independent biological repeat experiments. **K,** Immunohistochemistry staining of STAG1 in

engineered HCT-116 cells in absence and presence of Dox. Asterisk marks an area of murine fibroblasts that serve as an internal positive control. **I,** Growth curves of tumors implanted with engineered HCT 116 cells in the absence and presence of Dox.

Supplementary Figure 1 (related to figure 1) | Design and selection ARTi-shRNAmirs. A, Sequence logo displaying nucleotide position biases of seed sequences (guide position 2-8) with the lowest off-target score in siSPOTR analysis (top 1%). **B,** Sequence logo displaying position biases in sequences from a that harbor a T in guide position 2. **C,** Knockdown efficiency of ARTi-shRNAmirs. Flow cytometric quantification of GFP knockdown efficiency in immortalized MEFs two days after transduction with indicated ARTi-shRNAmir or control shRNAs. Percent knockdown is normalized to shRen.713 control. **D,** Toxicity of ARTi-shRNAmirs. Competitive proliferation assays of three murine cell lines after transduction with ARTi-shRNAmirs, shRen..713 or shMyc.1834 control. **E,** Principal component analysis of gene expression profiling in HT-1080 cells. Respective shRNAmirs and treatments are indicated in the respective colors. X-axis: principal component 1; Y-axis: principal component 2. **F,** Volcano plots visualizing de-regulated genes. All shRNAmirs and treatments were tested against the empty vector control. X-axis: $-\log_{10}$(p-value); Y-axis: $\log_2$ fold change. **G,** Cell growth assay for ARTi-shRNAmir transduced cells and their parental controls in the presence and absence of Dox.

Supplementary Figure 2 (related to figure 2) | Validation of ARTi *in vitro* and *in vivo* - EGFR. A, Functional validation of the $EGFR^{del19}$ construct in Ba/F3 cells. Provided are GI_{50} values (nM) for indicated conditions and compounds. Numbers represent GI_{50} value calculated from three technical repeats. Three biological repeat experiments were conducted, and one representative experiment is shown in panel A. **B,** Western Blot analysis confirming expression of $EGFR^{del19}$-ARTi constructs, knockout of endogenous EGFR and Dox-induced knockdown or $EGFR^{del19}$-ARTi. Western Blot is a representative example of three independent biological repeat experiments. **C,** Expression levels (y-axis: normalized counts) of the $EGFR^{del19}$-ARTi construct in parental and engineered PC-9 cells after 4 and 8 days of Dox treatment or no treatment. Individual datapoints of three biological replicates overlay the boxplots. **D,** Expression levels (y-axis: normalized counts) of DUSP6 in parental and engineered PC-9 cells after 4 and 8 days of Dox treatment or no treatment. Individual datapoints of three biological replicates overlay the boxplots. **E,** Heatmap visualizing the gene expression changes in MAPK pathway target and ERBB genes in engineered cells in the presence and absence of Dox. **F,** *In vivo* experiment comparing Dox-induced $EGFR^{del19}$-ARTi knockdown to drinking water control in PC-9 parental cells. Lines connect mean tumor volume data and +/- s.e.m..

Supplementary Figure 3 (related to figure 2) | Validation of ARTi *in vitro* and *in vivo* - KRAS. A, Schematic of MIA PaCa-2 genome engineering. **B,** AMG-510 GI_{50} values in MIA PaCa-2 parental and engineered cells. Numbers represent GI_{50} value calculated from three technical repeats. Three biological repeat experiments were conducted, and one representative experiment is shown in panel B. **C,** Expression levels (y-axis: normalized counts) of the dsRed::$KRAS^{G12R}$ transgene in parental and engineered MIA PaCa-2 cells after 4 and 8 days of Dox treatment or no treatment. Individual datapoints of three biological replicates overlay the boxplots. **D,** Western blot for KRAS (green) and Actin (magenta) (upper plot) and dsRed (green)

203 and Actin (magenta) (bottom plot) for indicated engineered MIA PaCa-2 cells in the presence and absence
204 of Dox. Western Blot is a representative example of three independent biological repeat experiments.

205

206 **Supplementary Figure 4 (related to figure 2) | Validation of ARTi *in vitro* and *in vivo* – STAG1. A,**
207 Schematic of synthetic lethal interaction between STAG1 and STAG2. Cells survive loss of either paralog
208 but are incapable of growing upon combined loss of STAG1 and STAG2. **B,** Western blot confirmation of
209 STAG2 knockout and ARTi-shRNAmir induced knockdown of endogenous STAG1::V5::ARTi. Western Blot
210 is a representative example of three independent biological repeat experiments. **C,** Proliferation assay of
211 ARTi engineered HCT 116 cells *in vitro*, visualized by crystal violet staining following a 9-day doxycycline
212 or control treatment. Staining is a representative example of three independent biological repeat
213 experiments. **D**, Quantification of nuclear Stag1 level (Figure 2k) using engineered HCT 116 cells in an in
214 vivo xenotransplantation experiment the control group (-dox) and doxycycline (+dox) treated group.

215

Material and Methods

Design and cloning of ARTi shRNAs

To design pairs of artificial shRNAs and matching target sites that trigger effective and selective target suppression with minimal off-target effects, nucleotide composition of shRNAs that reach exceptionally high performance scores in a well-established siRNA prediction tool (DSIR=Designer of Small Interfering RNA[9]) and contain no A or T in guide position 20 to eliminate shRNAmirs that produce RISC-loadable small RNAs from the passenger strand were analyzed. To establish criteria for ARTi design, siRNA predictions for the human and mouse genome were retrieved from DSIR[9] using default parameters. Top scoring predictions (DSIR score > 105) harboring G or C in position 20 were analyzed for nucleotide biases, which were used to define basic design criteria at the 5'-end the 3'-half. Next, possible off-targets were minimized using siSPOTR[10], an siRNA-based prediction tool that assesses off-target potential of different siRNA seed sequences (guide positions 2-8) in the human and mouse genome. Seed sequences with the lowest predicted off-target activity (top 1%) showed biases for C and/or G in guide positions 2-6, but 23% contained a T at the 5' end of the seed sequence that is required in our design (Fig. 1b). Among these, we observed particularly strong biases for CG in the following two positions (Fig. 1b), which were found in 73% of all seed sequences harboring a 5' T. Overall, 17% of all top-scoring seed sequences harbored TCG at their 5' end, making it the second most common triplet (after CGC, which was found in 20%). Based on these analyses, we fixed the first 4 nucleotides of the guide to TTCG. For the following positions we reasoned that introducing additional GC biases would destroy 5'-3' asymmetry of small RNA duplexes that is critically required for efficient RISC loading. To maintain sufficient asymmetry, we therefore decided to bias the next 3 positions towards A or T, which in most positions is in alignment with nucleotide biases associated with knockdown efficacy.

For the remaining sequence 3' of the seed region, we adhered to nucleotide features associated with knockdown efficacy based on our DSIR analysis, which are remarkably prominent and cannot all be explained through established processing requirements. Altogether, this established a 22-nt matrix for the design of ARTi shRNAmirs (TTCGWWWNNAHHWWCATCCGGN; W = A/T, H = A/T/C; N = A/T/G/C). In a last step, we further reduced possible off-target effects by eliminating all guides whose extended seed sequence (guide positions 2-14) had a perfect match in the human or mouse transcriptome and, finally, selected the following six top-scoring ARTi predictions for experimental validation:

ARTi.6588 – target site: TCCGGATGAAGTTTATATCGAA / shRNAmir (97mer):
TGCTGTTGACAGTGAGCGCCCGGATGAAGTTTATATCGAATAGTGAAGCCACAGATGTATTCGATATAAACTTCAT
CCGGATGCCTACTGCCTCGGA

ARTi.6570 – target site: TCCGGATGATATTGTTATCGAA / shRNAmir (97mer):
TGCTGTTGACAGTGAGCGCCCGGATGATATTGTTATCGAATAGTGAAGCCACAGATGTATTCGATAACAATATCAT
CCGGATGCCTACTGCCTCGGA

ARTi.6634 – target site: TCCGGATGATGTTTTAATCGAA / shRNAmir (97mer):
TGCTGTTGACAGTGAGCGCCCGGATGATGTTTTAATCGAATAGTGAAGCCACAGATGTATTCGATTAAAACATCAT
CCGGATGCCTACTGCCTCGGA

254 ARTi.6786 – target site: TCCGGATGATATTGTATACGAA / shRNAmir (97mer):
255 TGCTGTTGACAGTGAGCGCCCGGATGATATTGTATACGAATAGTGAAGCCACAGATGTATTCGTATACAATATCAT
256 CCGGATGCCTACTGCCTCGGA

257 ARTi.6834 – target site: TCCGGATGATATTGCATACGAA / shRNAmir (97mer):
258 TGCTGTTGACAGTGAGCGCCCGGATGATATTGCATACGAATAGTGAAGCCACAGATGTATTCGTATGCAATATCAT
259 CCGGATGCCTACTGCCTCGGA

260 ARTi.6516 – target site: TCCGGATGAAGTTTAATTCGAA / shRNAmir (97mer):
261 TGCTGTTGACAGTGAGCGCCCGGATGAAGTTTAATTCGAATAGTGAAGCCACAGATGTATTCGAATTAAACTTCAT
262 CCGGATGCCTACTGCCTCGGA

263

264 The following ARTi target sequences were used for experimental validation studies:

265 Insertion into the coding sequence before the STOP codon:

266 ATCCGGATGATATTGTATACGAATCCGGATGATATTGTTATCGAA (with the first "A" being inserted to retain
267 the reading frame)

268 Insertion after the STOP codon:

269 TCCGGATGATATTGTATACGAATCCGGATGATGTTTTAATCGAATCCGGATGATATTGTTATCGAA

270 shRNAs were ordered as single stranded DNA Ultramer oligonucleotides (Integrated DNA Technologies),
271 amplified by PCR and cloned into different retroviral or lentiviral miRE/miRF shRNAmir expression vectors
272 (LT3GFPIR[6]) using EcoR/XhoI restriction digest or Gibson assembly.

273

274 **Cell Culture**

275 Human HCT-116 cells (ATCC: CCL-247) were cultured in RPMI 1640 medium (Thermo Fisher) and PC-9 cells
276 in McCoy's 5A medium (Thermo Fisher), supplemented with 10% FBS and 1 x GlutaMAX (Thermo Fisher).
277 RKO (ATCC: CRL-2577) and MOLM-13 cells (DSMZ: ACC 584) were cultured in RPMI 1640, supplemented
278 with 10% FBS (Sigma-Aldrich), 4mM L-glutamine (Thermo Fisher), 1mM sodium pyruvate (Sigma-Aldrich),
279 and penicillin/streptomycin (100 U ml^{-1}/100 µg ml^{-1}, Sigma-Aldrich). HT-1080 (ATCC: CCL-121) and LentiX
280 lentiviral packaging cells (Clontech, cat. no. 632180) were cultivated in DMEM (Thermo Fisher) with 10%
281 FBS, 4mM L-glutamine, 1mM sodium pyruvate, and penicillin/streptomycin (100 U ml^{-1}/100 µg ml^{-1}).
282 MV4-11 cells (ATCC: CRL-9591) were cultured in IMDM with 10% FBS, 4mM L-glutamine, 1mM sodium
283 pyruvate, and penicillin/streptomycin (100 U ml^{-1}/100 µg ml^{-1}).

284 Murine MLL-AF9^{OE}, Nras^{G12D} AML cells (RN2; Zuber et al. 2011) were cultured in RPMI 1640 medium
285 supplemented with 10% FBS, 20 mM L-glutamine, 10 mM sodium pyruvate, 10 mM HEPES (pH 7.3),
286 penicillin/streptomycin (100 U ml^{-1}/100 µg ml^{-1}), and 50 µM β-ME. Kras^{G12D}, Trp53$^{-/-}$, MYC^{OE} PDAC cells
287 (EPP2), SV40 large T antigen immortalized mouse embryonic fibroblasts (RRT-MEF[22]; and NIH/3T3 (ATCC:
288 CRL-1658) were cultured in DMEM supplemented with 10% FBS, 20 mM glutamine, 10 mM sodium
289 pyruvate, and penicillin/streptomycin (100 U ml^{-1}/100 µg ml^{-1}). MIA PaCa-2 (ATCC: CRL-1420) and GP2d
290 (Ecacc: 95090714) cells were cultured in DMEM supplemented with 10% FBS. Ba/F3 (DSMZ: ACC300) cells
291 were cultured in RPMI 1640 medium supplemented with 10% FBS, 10ng/ml IL-3 (R&D systems) and Ls513

292 cells were cultured in RPMI 1640 medium supplemented with 10% FBS. All cell lines were maintained at
293 37°C with 5% CO_2, routinely tested for mycoplasma contamination and authenticated by short tandem
294 repeat analysis.

295

296 **Reporter Assay**

297 SFFV-GFP-P2A-Puro-ARTi-target sensor was cloned into pRSF91 retroviral plasmid[23] using Gibson
298 assembly. RRT-MEFs were transduced with retroviruses expressing a GFP-reporter harboring the target
299 sites for validated shRNAs and one ARTi-shRNA in its 3'-UTR. For each reporter cell line single cells were
300 FACS-sorted into 96-well plates using a FACSAria III cell sorter (BD Bioscience) to obtain single-cell derived
301 clones. These clones were transduced with retrovirus constructs in pSin-TRE3G-mCherry-miRE-PGK-Neo
302 (TCmPNe) backbone expressing either the respective doxycycline (Dox)-inducible ARTi shRNA or validated
303 shRNAs and mCherry fluorescence marker. shRNA expression was induced with Dox and GFP levels were
304 quantified via flow cytometry 2 days post induction. Knockdown efficiency was calculated as 1 minus the
305 ratio of mean GFP signal in $mCherry^+$ ($shRNA^+$) cells over $mCherry^-$ cells and normalized to Renilla
306 luciferase specific neutral control shRNA (Ren.713).

307

308 **Competitive proliferation assay**

309 To investigate the effect of ARTi constructs in the absence of the endogenous target gene, competitive
310 proliferation assays were performed in several human and murine cell lines. Human HT-1080, RKO,
311 MOLM-13, and MV4-11 cell lines were lentivirally transduced with shRNAmir expression constructs cloned
312 into pRRL-SFFV-GFP-miRF-PGK-Neo (SGFN) backbone at 20-60% efficiency. Initial infection efficiency was
313 determined at day 4 post transfection (day 0) by measuring GFP expression as a readout using iQue
314 Screener Plus flow cytometer (IntelliCyt). Percentage of $shRNA^+$ cells (GFP positive) was monitored by flow
315 cytometry in regular intervals and results were normalized to day 0.

316 Human GP2d, Ls513, and MIA PaCa-2 cell lines were lentivirally transduced with shRNAmir constructs
317 cloned into pRRL-TRE3G-GFP-miRE-PGK-Puro-IRES-rtTA3 backbone (LT3GEPIR, Addgene plasmid
318 #111177). 500 cells were seeded in duplicates in 96-well plates and treated with 1 µg/ml Dox for 9-10
319 days and analyzed with Incucyte (Sartorius). Untreated cells served as reference.
320 Murine NIH-3T3, EPP2 and RN2 cells were retrovirally transduced with shRNAmir constructs cloned into
321 pMSCV-miR-E-PGK-Neo-IRES-mCherry backbone (LENC; Addgene plasmid #111163), and initial infection
322 levels were determined by flow cytometry based on mCherry expression 4 days post transduction (day 0).
323

324 **Crystal Violet staining**

325 To visualize ARTi-shRNAmir's effect, crystal violet staining assays were performed. 25'000 HCT-116 cells
326 and 15'000 PC-9 cells per well were seeded in a 6-well plate containing 2 mL tetracycline-free growth
327 medium and 1 µg/mL Dox. Medium was exchanged every 2-3 days. After 9 days, wells were washed with
328 ice-cold PBS and subsequently stained with 1 mL of 2.3% crystal violet solution for 10 minutes.
329 Subsequently, wells were washed with ultrapure water and dried overnight. Images were obtained with
330 a scanner.

331
332
333 **Transcriptional profiling**

334 For the unbiased identification of ARTi shRNA off-targets, RKO and HT-1080 shRNA$^+$ cells from the
335 competition proliferative assay experiment were selected with Geneticin/G418 Sulfate (Gibco) for 7 days
336 and checked for GFP expression. On day 7, one arm of the empty vector control group was treated with
337 IC_{50} concentration of trametinib (MedChem Express: HY-10999) for 24 hours based on the data in
338 Genomics of Drug Sensitivity in Cancer (GDSC) database (https://www.cancerrxgene.org)[24]. Subsequently,
339 cells were trypsinized, washed with ice-cold PBS, pelleted and snap frozen. Total RNA was isolated using
340 in-house magnetic beads kit and King Fisher Duo Prime Purification System (Thermo Fisher). NGS libraries
341 were prepared with QuantSeq 3' mRNA-Seq Library Prep Kit (FWD) HT for Illumina (Lexogen) and UMI
342 Second Strand Synthesis Module for QuantSeq FWD (Lexogen). Samples were sequenced on Illumina
343 NovaSeq platform with 100bp single-read protocol.

344 Engineered MIA PaCa-2 and PC-9 cells were cultured in the presence of 1 µg/ml Dox to induce expression
345 of the ARTi shRNA. Dox-containing media were replenished twice weekly and on day 4 and day 8 after the
346 initial treatment. $2x10^6$ Dox-treated and untreated control cells were harvested, washed with PBS, lysed,
347 treated with DNAse I (QIAGEN) and total RNA was extracted using the RNeasy Mini Kit (QIAGEN). NGS
348 libraries were prepared as above. Samples were sequenced on an Illumina NextSeq 2000 platform with a
349 75bp protocol.
350
351 **Bioinformatic analyses of 3' mRNA-Seq**

352 For 3' mRNA-Seq reads derived from the human cell lines HT-1080 and RKO, the six nucleotide long 5'
353 UMIs were attached to each read name with umi-tools (v1.0.0)[25]. Subsequently, the UMIs plus the next
354 four nucleotides (UMI spacer), as well as 3' adapters (stringency of 3) and bases with low quality (threshold
355 of 25) were trimmed away using cutadapt (v1.18)[26] and its wrapper tool trimgalore (v0.6.2). Read quality
356 control was performed with FastQC (v0.11.8). The remaining reads were sample-wise aligned to the
357 human (GRCh38.p13; GCA_000001405.28) reference genome. Mapping and subsequent filtering of 3' UTR
358 mapped reads was performed with slamdunk (v0.4.3)[27] in QuantSeq mode (slamdunk map -5 12 -n 100 -
359 q). 3' UTR regions were assembled based on the description in Muhar et al.[28]. Aligned and filtered reads
360 were deduplicated with umi-tools (v1.0.0) (2), based on the mapping coordinate and the UMI attached to
361 the read name, prior to quantifying read abundances within 3' UTR regions using featureCounts (v2.0.1)[29].
362 Differential expression analysis (DEA) was performed with DESeq2 (v1.30.1)[30] for each ARTi shRNA to
363 empty vector control. Here, the number of up- and downregulated genes were calculated by filtering the
364 DEA results for genes with a log2 fold-change ≥ 2 (up) or ≤ 2 (down) and a -log10 p-value ≥ 5. Principal
365 component analysis was performed on the 1000 most variable expressed genes with the prcomp function
366 from the stats (v4.2.0) R package.

367 For transcriptional profiling of the human cell lines MIA-PaCa-2 and PC-9, the genome reference file and
368 annotations were constructed based on the GRCh38 assembly and the Ensembl 86 version, respectively.
369 The sequences of the shRNA construct (ARTi.6570 (RN_v_76, RN_v_118)) as well as the

370 EGFR^{del19}::V5::dsRed::ARTi (RN_v_108) and the dsRed::Linker::KRAS^{G12R}-ARTi (RN_v_287) were also
371 included. Mapping of the sequencing reads derived from the human cell lines was performed with STAR
372 (v2.5.2b)[31] aligner allowing for soft clipping of adapter sequences. Quantification of read counts to
373 transcript annotations was implemented using RSEM (v1.3.0)[32] and featureCounts (v1.5.1)[29].
374 Normalization of read counts and differential analysis was implemented with the limma[33] and voom[34] R
375 packages.
376

377 **Genome engineering of EGFR in PC-9 and Ba/F3**

378 Genome engineering of PC-9 cells was done as previously described[35]. In brief: PC-9_RIEN cells were
379 transduced with an ecotropic pMSCV-EGFRdel19_V5_dsRed_ARTi-PGK-Blasticidin retrovirus cloned at
380 GenScript and produced in Platinum E cells (Cell Biolabs) in the presence of 8 µg/mL Polybrene (Merck
381 Millipore). After 24 hours, stable transgenic cell pools were selected using 10 µg/mL Blasticidin (Sigma-
382 Aldrich). Subsequently, cells were diluted to obtain single cell clones. After 14 days of culture, single cell-
383 derived colonies were transferred to 6-well plates and analyzed by Western Blot. Identified homozygous
384 PC-9_ EGFR^{del19}-ARTi clones were further engineered by cutting endogenous EGFR with a CRISPR all-in-
385 one vector pX458_Exon20_gRNA `TAGTCCAGGAGGCAGCCGAA` (GenScript) using X-tremeGENE 9 DNA
386 transfection reagent (Roche) according to the protocol supplied by the vendor. 48 hours after
387 transfection, GFP positive cells were sorted by FACS (SONY cell sorter S800Z) and diluted to obtain single
388 cell clones. Positive clones, which contained only the exogenous EGFR^{del19}-ARTi, but not the endogenous
389 EGFR, were identified by Western Blot. Next, the selected EGFR clone was transduced with a pantropic
390 LT3GEPIR_Puro_ARTi-shRNA `TTCGATAACAATATCATCCGGA` retrovirus cloned at GenScript, China and
391 produced via the Lenti-X Single Shot system (Clontech). 72 hours later, stable transgenic cell pools were
392 selected using 0.5µg/mL Puromycin (Sigma-Aldrich). Following the selection, cells were diluted to obtain
393 single cell clones. After 14 days of culture, single cell-derived colonies were transferred to 6-well plates
394 and induced via 1µg/ mL Dox. Positive clones were characterized by a strong GFP-induction that was
395 identified by flow cytometry.
396

397 Ba/F3 cells were transduced with an ecotropic pMSCV-EGFRdel19_V5_dsRed_ARTi-PGK-Blasticidin
398 retrovirus cloned at GenScript and produced in Platinum E cells in the presence of 4 µg/mL Polybrene.
399 After 72 hours, stable transgenic cells were selected by using 50 µg/mL Blasticidin, without adding IL-3.
400

401 **Genome engineering of KRAS in MIA PaCa-2**

402 MIA PaCa-2 ARTi-shRNAmir expressing cells were transduced with an ecotropic pMSCV-dsRed::KRAS^{G12R}-
403 ARTi-PGK-Blasticidin retrovirus cloned at GenScript, China and produced in Platinum E cells in the
404 presence of 8 µg/mL Polybrene. After 24 hours, stable transgenic cell pools were selected using 10 µg/mL
405 Blasticidin. Subsequently, endogenous KRAS was knocked out by transient transfection of three gRNAs
406 targeting exon 2 and the region containing the G12C variant (present in MIA PaCa-2 cells) were used in a
407 co-transfection (gRNA#3: *GAATATAAACTTGTGGTAGT*; gRNA#6: *CTTGTGGTAGTTGGACTTG*; gRNA#7:
408 *GTAGTTGGAGCTTGTGGCGT*). Knockout clones were identified by the absence of the endogenous KRAS
409 protein using Western Blot.

410

411 **Genome engineering of STAG1/STAG2 in HCT-116**

412 HCT-116 cell line was engineered by cutting STAG1 with gRNAs targeting the region close to the STOP
413 codon. Guide RNAs *TTCTTCAGACTTCAGAACAT* or *CTGAAGAAAATTTACAAATC* were cloned into the
414 pSpCas9(BB)-2A-GFP plasmid (pX458; Addgene plasmid 48138) and used in a co-transfection.
415 Simultaneously, a STAG1_AID_V5_P2A_Blasti_STOP_ARTi repair template with 800bp of left and right
416 homologous arms of the STAG1 genomic locus (in pUC57-Simple backbone) was transfected into HCT-116
417 cells using Lipofectamine 3000 transfection reagent (Thermo Fisher) according to the manufacturer's
418 instructions. A stable transgenic cell pool was selected 48 hours after transfection using 5µg/ml Blasticidin
419 and diluted to obtain single cell clones. Positive clones were identified by Western Blot.

420 Identified homozygous HCT-116_STAG1_ARTi clones were further engineered by disrupting STAG2 gene
421 with a CRISPR all-in-one vector Hs0000077505_U6gRNA-Cas9-2A-GFP and Hs0000077502_U6gRNA-Cas9-
422 2A-GFP, respectively. Cells were transfected using X-tremeGENE 9 DNA transfection reagent according to
423 the manufacturer's instructions, sorted 48 hours post transfection for GFP positive cells and diluted to
424 obtain single cell clones. Positive clones were identified by Western Blot.

425 Next, the selected HCT-116 clone was transduced with a pantropic LT3GEPIR_Puro_ARTi-shRNA
426 *TTCGATAACAATATCATCCGGA* retrovirus cloned at GenScript, China and produced via the Lenti-X Single
427 Shot system (Clontech). 72 hours later, stable transgenic cell pools were selected using 2 µg/mL Puromycin
428 (SIGMA, P9620). Following the selection, cells were diluted to obtain single cell clones. After 14 days of
429 culture, single cell-derived colonies were transferred to 6-well plates and induced via 1µg/ mL Dox.
430 Positive clones were characterized by a strong GFP-induction that was identified by flow cytometry.
431

432 **Western Blot**

433 The following primary antibodies were used for immunoblot analyses: EGFR (Cell Signaling, #4267); STAG1
434 (GeneTex, GTX129912); STAG2 (Bethyl, A300-159A); b-actin (Sigma, A5441); KRAS (LSbio, LS-C17566); V5
435 (Sigma, V8012). PC-9, MIA PaCa-2, and HCT-116 cell pellets harboring EGFR, KRAS, and STAG1/STAG
436 constructs respectively were lysed in Triton X-100 lysis buffer, sonicated and stored at -80°C. For protein
437 detection, the pellets were thawed on ice, followed by 15 minutes centrifugation at 13,000 rpm and 4°C.
438 Further, cell lysates were loaded onto a pre-casted SDS–polyacrylamide gel (4-12%) and proteins were
439 transferred onto a nitrocellulose or PVDF-membrane. Membranes were probed with the respective
440 primary antibodies overnight. The next day, secondary antibodies conjugated with fluorescent dye were
441 added and the proteins were detected by the Odyssey detection system.
442

443 **Compound treatment**

444 To investigate sensitivity to EGFR-targeting compounds, cell viability was determined using the Cell Titer
445 Glo assay (Promega). For this purpose, 10 mM stock solutions in DMSO of afatinib[36], Osimertinib[37,38] [37]
446 and poziotinib[39,40] were used. 5'000 cells per well were seeded in 150µL of the medium in technical
447 triplicates in 96-well plates and incubated at 37°C and 5% CO_2 for 5 hours, followed by the compound
448 addition. Cells were treated with seven different concentrations of inhibitors in a serial eight-fold dilutions
449 starting with the highest concentration of 3 µM. For comparability, DMSO normalization to the highest
450 added volume was performed. Subsequently, cells were cultivated for 96 hours at 37°C and 5% CO_2. 50 µL
451 of Cell Titer Glo reagent was added to each well, incubated for 10 minutes in the dark and luminescence

452 was measured using the multilabel Plate Reader VICTOR X4. The measurement time was set to 0.2
453 seconds. Luminescence values relative to DMSO-treated cells were plotted in GraphPad Prism and fitted
454 using nonlinear regression with a variable slope to calculate IC50 values at 50% inhibition. MIA PaCa-2
455 KRAS G12C inhibitor (AMG-510)[17–19] treatments were performed as described for EGFR with the following
456 modifications: 2'000 cells per well, and 0.5nM-3µM concentration range of AMG-510.

457

458 ***In vivo* experiments**

459 The PC-9 EGFR k.o., EGFR^{del19}::ARTi study was performed at the AAALAC accredited animal facility of
460 CrownBio Leicestershire, UK. Female NSG® (NOD.Cg-PrkdcscidIl2rgtm1wjl/SzJ) Crl mice were obtained
461 from Charles River. Age of animals at study initiation was 7-8 weeks and hat an acclimatization period of
462 ≥14 days. Mice were groups housed in IVCs. The study complies with the UK Animals Scientific Procedures
463 Act 1986 (ASPA) in line with Directive 2010/63/EU of the European Parliament and the Council of 22
464 September 2010 on the protection of animals used for scientific purposes.

465 All other in vivo experiments were performed at the AAALAC accredited animal facility of Boehringer
466 Ingelheim RCV GmbH & CoKG. Female BomTac:NMRI-*Foxn1^{nu}* mice were obtained from Taconic Denmark
467 at 6-8 weeks of age. After the arrival, mice were allowed to adjust to the housing conditions at least for 5
468 days before the start of the experiment. Mice were housed in pathogen-free and controlled
469 environmental conditions (open cage housing), and handled according to the institutional, governmental
470 and European Union guidelines (Austrian Animal Protection Laws, GV-SOLAS and FELASA guidelines).

471 Studies were approved by the internal ethics committee (called "ethics committee") of Boehringer
472 Ingelheim RCV GmbH & Co KG in the department of Cancer Pharmacology and Disease Positioning.
473 Furthermore, all protocols were approved by the Austrian governmental committee (MA 60 Veterinary
474 office; approval numbers GZ: 903122/2017/21 and GZ: 416181-2020-29).

475 To establish subcutaneous tumors, mice were injected with 2 x 10^6 HCT-116 in PBS, 5 x 10^6 MIA PaCa-2
476 in 1:2 Matrigel : PBS with 5% FBS or with 1 x 10^7 PC-9 cells in PBS with 5% FBS.

477 Tumor diameters were measured with a caliper three times a week. The volume of each tumor [in mm^3]
478 was calculated according to the formula "tumor volume = length * diameter^2 * π/6." Mice were
479 randomized into the treatment groups when tumor size reached between ~130 and 190 mm^3. Group sizes
480 were calculated for each tumor model based on tumor growth during model establishment experiments.
481 A power analysis was performed using a sample size calculator
482 (https://www.stat.ubc.ca/~rollin/stats/ssize/n2.html). For all models used in the studies, 10 mice per
483 group were used. 2mg/ml Doxycycline hyclate (Sigma) and 5mg/ml sucrose were added to the drinking
484 water of the treatment groups, the control group received water with 5mg/ml sucrose only. Osimertinib
485 (Tagrisso, AstraZeneca, 40 mg tablet) was dosed per os daily at a dose of 25mg/kg in Natrosol and control
486 mice were dosed per os daily with Natrosol. To monitor side effects of treatment, mice were inspected
487 daily for abnormalities and body weight was determined three times per week. Animals were sacrificed
488 when the tumors reached a size of 1'500 mm^3. Food and water were provided ad libitum. *In vivo*
489 experiments were not repeated.

490

491 **Immunohistochemistry**

492 Xenograft samples were fixed in 4% formaldehyde for 24 h and embedded in paraffin. Two-micrometer-
493 thick sections were cut using a microtome. STAG1 was stained with Polink 2 Plus HRP rat NM detection
494 system (GBI Labs #D46-6) according to manufacturer's instructions using a recombinant rat monoclonal
495 STAG1 antibody (Abcam ab241544, Lot:GR3334172-1; 1:200) after cooking 10 minutes at 110°C in
496 antigen unmasking solution (Vector #H3301). After staining the slides were digitalized (scanner: Leica
497 Aperio AT2). All slides were reviewed and evaluated for quality by a board-certified MD Pathologist.
498 Imaging analysis was performed using the digital pathology platform HALO (Indica Labs). A tissue-
499 classifying algorithm was trained to selectively recognize viable tumor tissue against stroma, necrosis,
500 and skin. The tissue classification output for each scan was reviewed and manually edited as necessary.
501 A cell detection and scoring algorithm was trained to measure DAB optical density (OD) in the nuclei of
502 tumor cells. A positivity threshold for DAB OD was determined by normalization with respect to the DAB
503 OD as calculated from *bona fide* negative tissue (e.g., murine stroma as background). The object data for
504 background-normalized nuclear ODs for each tumor cell were exported from three control and three
505 doxycycline-treated cases (207945 and 33331 pooled objects, respectively). The cumulative distribution
506 of the background-normalized DAB OD for each tumor cell nucleus was then plotted for control and
507 doxycycline-treated cases, separately (supplemental figure 4, panel K).

508

509 **Reagents, code and data availability**

510 DNA sequences of the transgenes used in this study and the code used to generate the figures are
511 available upon request. The workflow for the RNA-seq bioinformatics analyses is described in the
512 Materials and Methods section. RNA sequencing data were uploaded to GEO with the accession
513 numbers: GSE218404 and GSE218617. The data will be made publicly available upon acceptance of this
514 manuscript. All ARTi cell lines and constructs described in this study are available upon request.

515

516 **Cell lines**

517 All newly generated ARTi cell lines are available upon request. The following parental cell lines were
518 used:

519

Cell line name	species	Supplier name	Catalog number	Clone number
PC-9	human	ECACC	90071810	Lot# 14A030
MIA PaCa 2	human	ATCC	CRL-1420	Lot# 1350798
HT 1080	human	ATCC	CCL-121	Lot# 63835574
HCT 116	human	ATCC	CCL-247	Lot# 6028631
RKO	human	ATCC	CRL-2577	Lot# 59354083
MV4-11	human	ATCC	CRL-9591 (old number)	Lot# 58352230
MOLM-13	human	DSMZ	ACC 554	Lot# 11
NIH-3T3	human	ATCC	CRL-1658	Lot# 63292276

EPP2		$Kras^{G12D}$, $Trp53^{-/-}$, MYC^{OE} PDAC cells (EPP2)	NA	NA
RN2	murine	MLL-$AF9^{OE}$, $Nras^{G12D}$ AML cells (RN2; Zuber et al. 2011)	NA	NA
Gp2d	human	ECACC	95090714	Lot# 11E013
Ls513	human	ATCC	CRL-2134	Lot# 57761342
Ba/F3	murine	DSMZ	ACC300	
293T-Lenti-X	human	Clontech	632180	Lot# 1404558A

Competing interests

Alexandra Hörmann, Maja Corcokovic, Jasko Salkanovic, Fiona Spreitzer, Anna Köferle, Katrin Gitschtaler, Alexandra Popa, Sarah Oberndorfer, Nicole Budano, Jan G. Ruppert, Paolo Chetta, Melanie Wurm and Ralph Neumüller: Full time employees Boehringer Ingelheim RCV. Johannes Zuber: Quantro Therapeutics GmbH (Co-founder, Scientific Advisor, Shareholder); Mirimus Inc. (Scientific Advisor, Shareholder); AstraZeneca-CRUK Functional Genomics Consortium (Scientific Advisor); Boehringer Ingelheim (Research Support).

Funding

Ja.Z. is supported by the Swiss National Science Foundation (Early Postdoc Mobility Fellowship P2BSP3_188110) and European Union's Horizon 2020 research and innovation program under the Marie Skłodowska-Curie grant agreement No. 847548 (VIP2) and No. 101032582 (AML-SynergyX). Research at the IMP is supported by Boehringer Ingelheim and the Austrian Research Promotion Agency (Headquarter grant FFG-852936).

536 ## References

537

538 1. Mohr, S. E., Smith, J. A., Shamu, C. E., Neumüller, R. A. & Perrimon, N. RNAi screening comes of age:
539 improved techniques and complementary approaches. *Nat Rev Mol Cell Bio* 15, 591–600 (2014).

540 2. Housden, B. E. *et al.* Loss-of-function genetic tools for animal models: cross-species and cross-
541 platform differences. *Nat Rev Genet* 18, 24–40 (2017).

542 3. Jackson, A. L. *et al.* Expression profiling reveals off-target gene regulation by RNAi. *Nat Biotechnol* 21,
543 635–637 (2003).

544 4. Scacheri, P. C. *et al.* Short interfering RNAs can induce unexpected and divergent changes in the levels
545 of untargeted proteins in mammalian cells. *P Natl Acad Sci Usa* 101, 1892–1897 (2004).

546 5. Lin, X. *et al.* siRNA-mediated off-target gene silencing triggered by a 7 nt complementation. *Nucleic*
547 *Acids Res* 33, 4527–4535 (2005).

548 6. Fellmann, C. *et al.* An Optimized microRNA Backbone for Effective Single-Copy RNAi. *Cell Reports* 5,
549 1704–1713 (2013).

550 7. Premsrirut, P. K. *et al.* A Rapid and Scalable System for Studying Gene Function in Mice Using
551 Conditional RNA Interference. *Cell* 145, 145–158 (2011).

552 8. Zuber, J. *et al.* Toolkit for evaluating genes required for proliferation and survival using tetracycline-
553 regulated RNAi. *Nat Biotechnol* 29, 79–83 (2011).

554 9. Vert, J.-P., Foveau, N., Lajaunie, C. & Vandenbrouck, Y. An accurate and interpretable model for siRNA
555 efficacy prediction. *Bmc Bioinformatics* 7, 520 (2006).

556 10. Boudreau, R. L. *et al.* siSPOTR: a tool for designing highly specific and potent siRNAs for human and
557 mouse. *Nucleic Acids Res* 41, e9–e9 (2013).

558 11. Hynes, N. E. & MacDonald, G. ErbB receptors and signaling pathways in cancer. *Curr Opin Cell Biol*
559 21, 177–184 (2009).

560 12. Punekar, S. R., Velcheti, V., Neel, B. G. & Wong, K.-K. The current state of the art and future trends in
561 RAS-targeted cancer therapies. *Nat Rev Clin Oncol* 1–19 (2022) doi:10.1038/s41571-022-00671-9.

562 13. Bailey, M. L. *et al.* Paralogous synthetic lethality underlies genetic dependencies of the cancer-
563 mutated gene STAG2. *Life Sci Alliance* 4, e202101083 (2021).

564 14. Lelij, P. van der *et al.* STAG1 vulnerabilities for exploiting cohesin synthetic lethality in STAG2-
565 deficient cancers. *Life Sci Alliance* 3, e202000725 (2020).

566 15. Benedetti, L., Cereda, M., Monteverde, L., Desai, N. & Ciccarelli, F. D. Synthetic lethal interaction
567 between the tumour suppressor STAG2 and its paralog STAG1. *Oncotarget* 5, 37619–37632 (2014).

568 16. Lelij, P. van der *et al.* Synthetic lethality between the cohesin subunits STAG1 and STAG2 in diverse
569 cancer contexts. *Elife* 6, e26980 (2017).

570 17. Fakih, M. *et al.* CodeBreak 100: Activity of AMG 510, a novel small molecule inhibitor of KRAS G12C ,
571 in patients with advanced colorectal cancer. *J Clin Oncol* 38, 4018–4018 (2020).

572 18. Lanman, B. A. *et al.* Discovery of a Covalent Inhibitor of KRASG12C (AMG 510) for the Treatment of
573 Solid Tumors. *J Med Chem* 63, 52–65 (2020).

574 19. Fakih, M. *et al.* Phase 1 study evaluating the safety, tolerability, pharmacokinetics (PK), and efficacy
575 of AMG 510, a novel small molecule KRAS G12C inhibitor, in advanced solid tumors. *J Clin Oncol* 37,
576 3003–3003 (2019).

577 20. Lai, A. C. & Crews, C. M. Induced protein degradation: an emerging drug discovery paradigm. *Nat Rev*
578 *Drug Discov* 16, 101–114 (2017).

579 21. Cromm, P. M. & Crews, C. M. Targeted Protein Degradation: from Chemical Biology to Drug
580 Discovery. *Cell Chem Biol* 24, 1181–1190 (2017).

581 22. Fellmann, C. *et al.* Functional Identification of Optimized RNAi Triggers Using a Massively Parallel
582 Sensor Assay. *Mol Cell* 41, 733–746 (2011).

583 23. Galla, M. *et al.* Avoiding cytotoxicity of transposases by dose-controlled mRNA delivery. *Nucleic Acids*
584 *Res* 39, 7147–7160 (2011).

585 24. Yang, W. *et al.* Genomics of Drug Sensitivity in Cancer (GDSC): a resource for therapeutic biomarker
586 discovery in cancer cells. *Nucleic Acids Res* 41, D955–D961 (2013).

587 25. Smith, T., Heger, A. & Sudbery, I. UMI-tools: modeling sequencing errors in Unique Molecular
588 Identifiers to improve quantification accuracy. *Genome Res* 27, 491–499 (2017).

589 26. Martin, M. Cutadapt removes adapter sequences from high-throughput sequencing reads. *Embnet J*
590 17, 10–12 (2011).

591 27. Neumann, T. *et al.* Quantification of experimentally induced nucleotide conversions in high-
592 throughput sequencing datasets. *Bmc Bioinformatics* 20, 258 (2019).

593 28. Muhar, M. *et al.* SLAM-seq defines direct gene-regulatory functions of the BRD4-MYC axis. *Science*
594 360, 800–805 (2018).

595 29. Liao, Y., Smyth, G. K. & Shi, W. featureCounts: an efficient general purpose program for assigning
596 sequence reads to genomic features. *Bioinformatics* 30, 923–930 (2014).

597 30. Love, M. I., Huber, W. & Anders, S. Moderated estimation of fold change and dispersion for RNA-seq
598 data with DESeq2. *Genome Biol* 15, 550 (2014).

599 31. Dobin, A. *et al.* STAR: ultrafast universal RNA-seq aligner. *Bioinformatics* 29, 15–21 (2013).

600 32. Li, B. & Dewey, C. N. RSEM: accurate transcript quantification from RNA-Seq data with or without a
601 reference genome. *Bmc Bioinformatics* 12, 323 (2011).

602 33. Ritchie, M. E. *et al.* limma powers differential expression analyses for RNA-sequencing and
603 microarray studies. *Nucleic Acids Res* 43, e47–e47 (2015).

604 34. Law, C. W., Chen, Y., Shi, W. & Smyth, G. K. voom: precision weights unlock linear model analysis
605 tools for RNA-seq read counts. *Genome Biol* 15, R29–R29 (2014).

606 35. Wilding, B. *et al.* Discovery of potent and selective HER2 inhibitors with efficacy against HER2 exon
607 20 insertion-driven tumors, which preserve wild-type EGFR signaling. *Nat Cancer* 3, 821–836 (2022).

608 36. Li, D. *et al.* BIBW2992, an irreversible EGFR/HER2 inhibitor highly effective in preclinical lung cancer
609 models. *Oncogene* 27, 4702–4711 (2008).

610 37. Liu, S. *et al.* Targeting HER2 Aberrations in Non–Small Cell Lung Cancer with Osimertinib. *Clin Cancer*
611 *Res* 24, 2594–2604 (2018).

612 38. Soria, J.-C. *et al.* Osimertinib in Untreated EGFR -Mutated Advanced Non–Small-Cell Lung Cancer.
613 *New Engl J Med* 378, 113–125 (2018).

614 39. Kim, T.-Y. *et al.* A phase I/II study of poziotinib combined with paclitaxel and trastuzumab in patients
615 with HER2-positive advanced gastric cancer. *Gastric Cancer* 22, 1206–1214 (2019).

616 40. Robichaux, J. P. *et al.* Pan-Cancer Landscape and Analysis of ERBB2 Mutations Identifies Poziotinib as
617 a Clinically Active Inhibitor and Enhancer of T-DM1 Activity. *Cancer Cell* 36, 444-457.e7 (2019).

618

Design and selection of ARTi-shRNAmirs

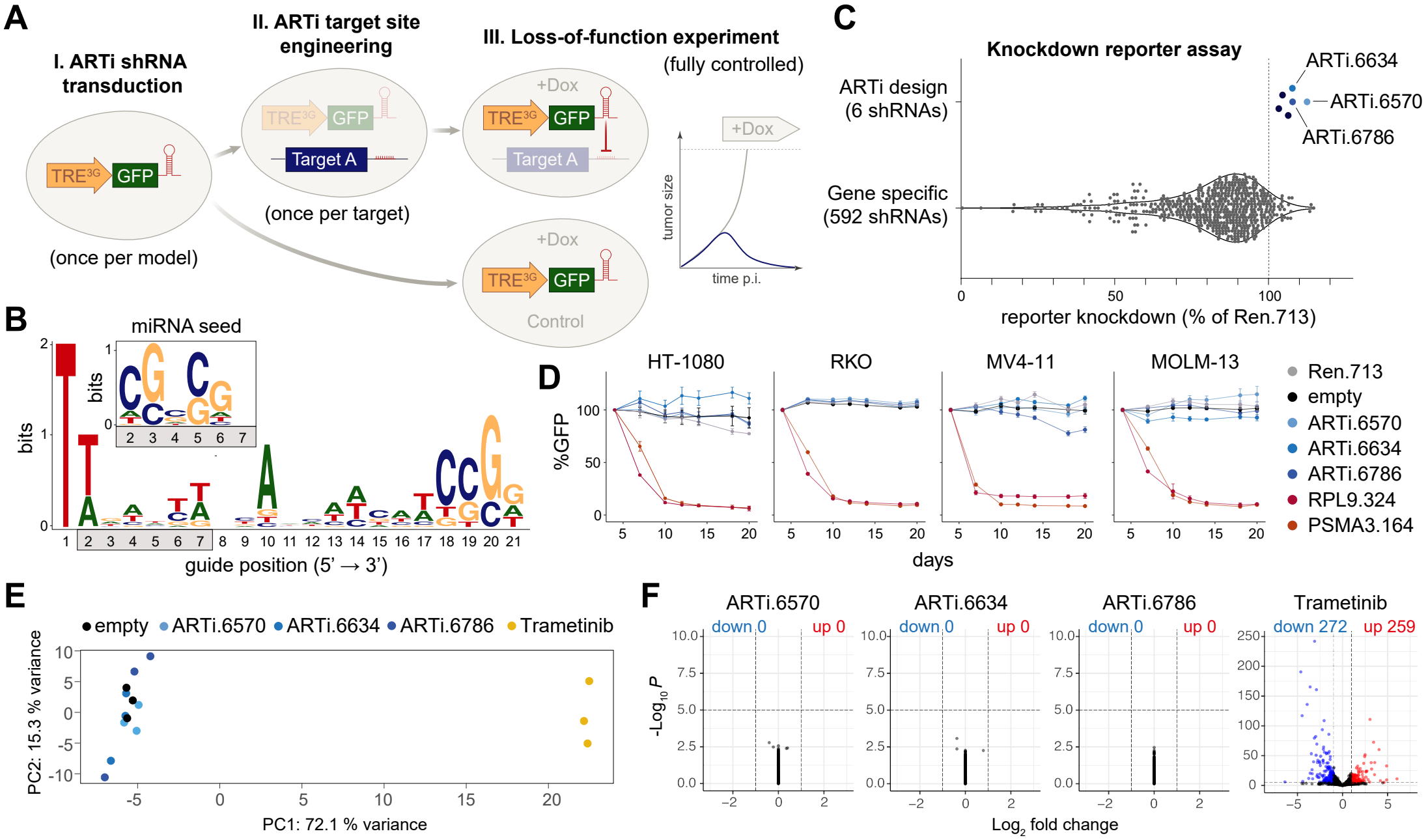

Hoffmann et al., Figure 1

Experimental validation of the ARTi approach

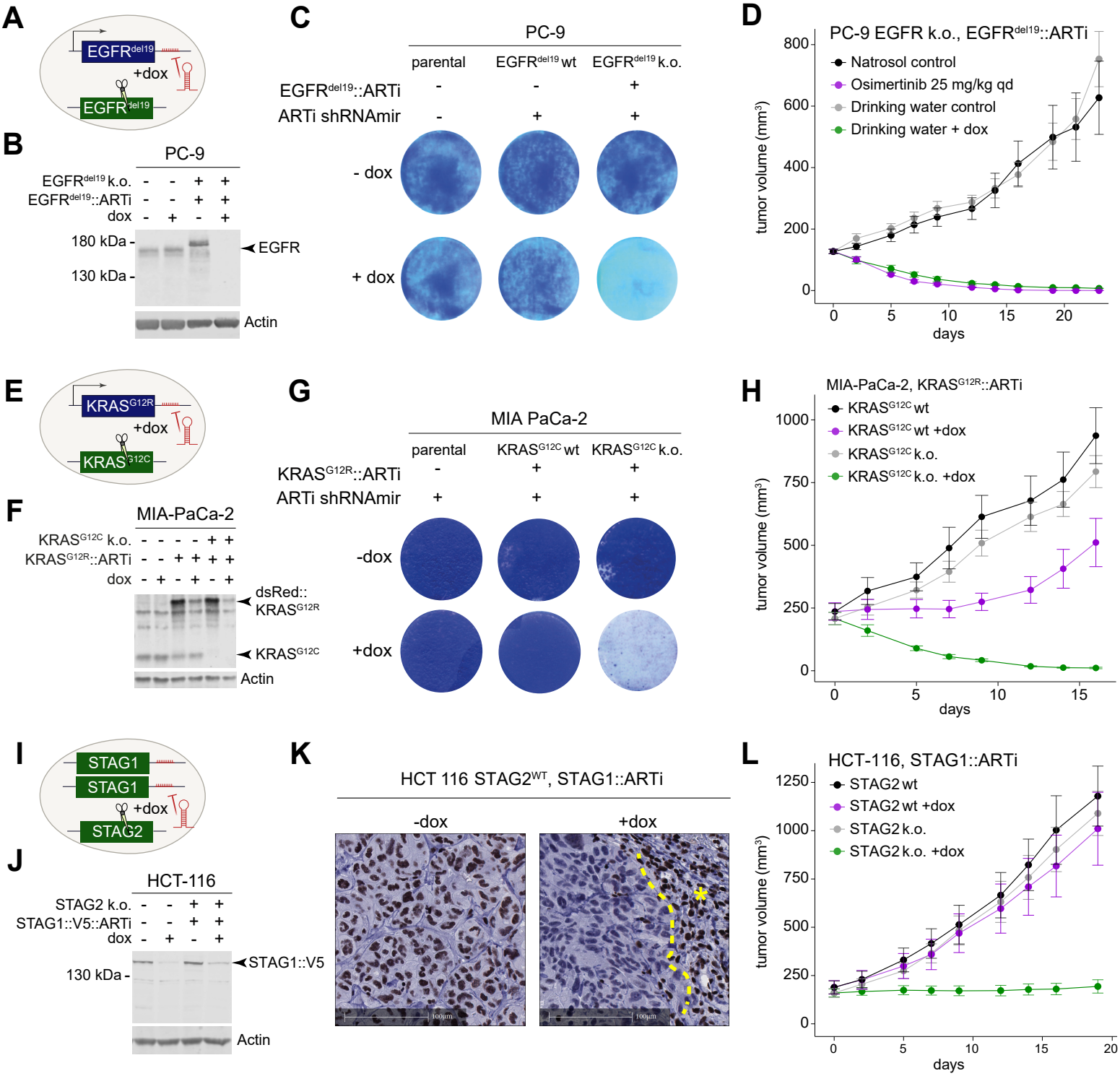

Hoffmann et al., Figure 2